

Memory-multi-fractional Brownian motion with continuous correlations

Wei Wang,¹ Michał Balcerek,² Krzysztof Burnecki,² Aleksei V. Chechkin,^{1,2,3} Skirmantas Janušonis,⁴ Jakub Ślęzak,² Thomas Vojta,⁵ Agnieszka Wyłomańska,² and Ralf Metzler^{1,6}

¹*Institute of Physics & Astronomy, University of Potsdam, 14476 Potsdam, Germany*

²*Faculty of Pure and Applied Mathematics, Hugo Steinhaus Center,
Wrocław University of Science and Technology, Wrocław, Poland*

³*Akhiezer Institute for Theoretical Physics, National Science Center
"Kharkov Institute of Physics and Technology", Kharkov 61108, Ukraine*

⁴*Department of Psychological and Brain Sciences,
University of California, Santa Barbara, Santa Barbara, CA 93106, USA*

⁵*Department of Physics, Missouri University of Science and Technology, Rolla, MO 65409, USA*

⁶*Asia Pacific Center for Theoretical Physics, Pohang 37673, Republic of Korea*

(Dated: 4th August 2023)

We propose a generalization of the widely used fractional Brownian motion (FBM), memory-multi-FBM (MMFBM), to describe viscoelastic or persistent anomalous diffusion with time-dependent memory exponent $\alpha(t)$ in a changing environment. In MMFBM the built-in, long-range memory is continuously modulated by $\alpha(t)$. We derive the essential statistical properties of MMFBM such as response function, mean-squared displacement (MSD), autocovariance function, and Gaussian distribution. In contrast to existing forms of FBM with time-varying memory exponents but reset memory structure, the instantaneous dynamic of MMFBM is influenced by the process history, e.g., we show that after a step-like change of $\alpha(t)$ the scaling exponent of the MSD after the α -step may be determined by the value of $\alpha(t)$ before the change. MMFBM is a versatile and useful process for correlated physical systems with non-equilibrium initial conditions in a changing environment.

PACS numbers: 87.15.Vv, 87.16.dp, 82.56.Lz, 05.40.-a, 02.50.-r

The stochastic motion of individual colloidal particles or labeled single molecules is routinely recorded by single-particle tracking [1] in soft- and bio-matter systems [2–4], i.e., crowded liquids [5, 6], cytoplasm of biological cells [7–11], actively driven tracers [12–14], lipid membranes [15–17], and porous media [18]. In silico, lipid and protein motion [19–21] or internal protein dynamics [21, 22] are sampled. On larger scales, motile cells or small organisms [23–25], and animals, e.g., marine predators or birds [26–30] are traced. Often the observed motion deviates from Brownian motion with its linear mean-squared displacement (MSD) $\langle x^2(t) \rangle \simeq t$ and Gaussian displacement probability density function (PDF) [31]. Instead, anomalous diffusion with MSD $\langle x^2(t) \rangle \simeq t^\alpha$ emerges [2–4], with sub- ($0 < \alpha < 1$) and superdiffusion ($\alpha > 1$) [2, 32]. Depending on the system, anomalous diffusion is described by different generalized stochastic models [32–36].

Two such processes have turned out to be particularly suited to model anomalous diffusion in a wide range of systems. One is the continuous time random walk, in which (waiting) times τ between two successive jumps are randomly distributed [32–34]. When the PDF of τ has the scale-free form $\psi(\tau) \simeq \tau^{-1-\alpha}$ with $0 < \alpha < 1$, the resulting motion is subdiffusive [32–34]. Power-law forms for $\psi(\tau)$ were, i.e., measured for colloids in actin gels [37, 38], membrane channels [15], doxorubicin molecules in silica slits [39], ribonucleoproteins in neurons [40], foraging birds [30], or in weakly chaotic systems [41, 42].

The second common anomalous diffusion process is fractional Brownian motion (FBM) [43, 44] based on

the stochastic equation $dX(t)/dt = \xi(t)$ driven by fractional Gaussian noise (FGN) with stationary autocovariance function (ACVF) $\langle \xi(t)\xi(t+\tau) \rangle \sim \frac{1}{2}\alpha(\alpha-1)K_\alpha\tau^{\alpha-2}$ ($0 < \alpha \leq 2$) [45, 46]. Then, $\langle X^2(t) \rangle \simeq K_\alpha t^\alpha$ with the generalized diffusivity K_α of dimension length²/time ^{α} . The ACVF is negative (“antipersistent”) for subdiffusion and positive (“persistent”) for superdiffusion. Displacement ACVFs consistent with sub- and superdiffusive FBM were identified, i.e., for tracers in crowded liquids [5–9, 47–50], doxorubicin [39], lipids [19], amoeba motion [47, 48], and cruising birds [30]. Specifically, subdiffusive FBM models diffusion in viscoelastic systems (cellular cytoplasm, crowded liquids) [5–9, 19], due to hydrodynamic backflow [51–54], or “roughness” in finance [55, 56]. FBM is intrinsically Gaussian [43–45], yet, in several viscoelastic systems non-Gaussian displacement PDFs were found [8, 16, 20, 49, 50]. This phenomenon (similar to Brownian yet non-Gaussian diffusion [57, 58]) was ascribed to the systems’ heterogeneity and modeled by superstatistical viscoelastic motion [59], FBM switching between two diffusivities [49] or featuring a stochastic (“diffusing” [60, 61]) diffusivity [62, 63], and subordinated FBM [50]. Random anomalous memory exponents α were studied in particle ensembles [64, 65].

Here we address systems in which the properties of long-range correlated motions do not vary stochastically but the memory exponent α changes deterministically over time, $\alpha(t)$. Examples include smoothly changing viscoelastic environments, e.g., during biological cell cycles [66], or when pressure and/or concentra-

tions are changed in viscoelastic solutions [67, 68]. $\alpha(t)$ may switch more abruptly when the test particle moves across boundaries to a different environment. Jump-like changes of α may be effected by binding to larger objects or surfaces [49, 69] or multimerization [69, 70] of the tracer. Drops in α from superdiffusion with $\alpha \approx 1.8$ to strong subdiffusion $\alpha \approx 0.2$ of intracellular particles were effected by blebbistatin treatment knocking out active molecular motor action in amoeba cells; after some time, the positive correlations and thus superdiffusion were restored [47]. Cellular sub-micron or micron-sized “cargo” transported by molecular motors may switch between motor-driven transport and rest phases, effecting repeated sub/superdiffusive switches [71, 72]. Finally, crossovers between sub/superdiffusive modes as well as changes in exponents within sub- or superdiffusion may occur for (intermittent) search of birds or other animals. We model such situations by a specified protocol $\alpha(t)$ for the memory exponent in our memory-multi-FBM (MMFBM) model, in which the memory of MMFBM is continuously modulated by $\alpha(t)$. Due to the uninterrupted memory, the instantaneous dynamic of MMFBM is influenced by the full history of the process. We study these memory effects on trajectories, response function, MSD, and ACVF. We show that MMFBM is Gaussian and discuss relations to other generalized FBM models.

To motivate our approach, consider the simple case of a Brownian particle with diffusivity K_1 , released at time $t = 0$. At time $t = \tau$ it switches to a new diffusivity K_2 , e.g., by crossing to a different environment, multimerization [70], or conformational changes [21]. The MSD of this particle has the form $\langle x^2(t) \rangle = 2K_1t$ for $t \leq \tau$ and $= 2K_2(t - \tau) + 2K_1\tau$ for $t > \tau$. A convenient way to formulate such types of processes is based on the Wiener process $B(t)$ [31] using $\tilde{B}(t) = \int_0^t \sqrt{K(s)} dB(s)$. In this formulation $K(s)$ continuously modulates the Wiener increments $dB(s)$ and, e.g., leads to above MSD.

In a similar fashion we incorporate a time-dependent memory exponent $\alpha(t)$ in FBM. For a physical process initiated at $t = 0$ we use Lévy’s formulation [73] of non-equilibrated FBM in terms of a (Holmgren) Riemann-Liouville fractional integral (RL-FBM) [44, 74],

$$X(t) = \int_0^t \sqrt{\alpha(s)} (t-s)^{(\alpha(s)-1)/2} dB(s). \quad (1)$$

In standard RL-FBM, the power-law memory kernel with constant exponent α modulates the Wiener increments $dB(s)$ along the path and at long times is equivalent to integrated FGN. Thus, at any point the process $X(t)$ depends on its full history. For $\alpha = 1$ the kernel vanishes and $X(t)$ is Brownian motion [44]. For changing environments MMFBM incorporates these changes locally into the memory function, i.e., by variation of how the correlations of the Wiener increments $dB(s)$ are modulated by $\alpha(s)$ along the path. Thus the uninterrupted history of $\alpha(t)$ is contained yet the strength of the memory varies

throughout the process history. We note that due to the explicit time dependence of $\alpha(t)$ the noise ACVF is by construction not stationary. We also note that the structure (1) for $X(t)$ is similar to time-fractional dynamics of CTRWs with scale-free waiting time PDF [33] and extensions to variable-order with time-dependent memory exponent [75]. We show that MMFBM with its statistical observables is a meaningful generalization of FBM.

Response function. We consider MMFBM (1), that is originally Brownian (i.e., $\alpha = 1$) up to time τ and then experiences a short period δ with exponent $\alpha \neq 1$. After $t = \tau + \delta$, the process is again Brownian. With the increments $X^\delta(\tau) = X(\tau + \delta) - X(\tau)$ the response function is

$$\langle X^\delta(\tau) X^\delta(\tau+T) \rangle = \alpha \delta \frac{\alpha-1}{2T^{1-\alpha}} B\left(\frac{\delta}{T}; \frac{\alpha+1}{2}, 1-\alpha\right) \quad (2)$$

for $\delta \rightarrow 0$, at time T after start of the perturbation with α [76]. B is the incomplete Beta function. When $T \rightarrow \infty$, $\langle X^\delta(\tau) X^\delta(\tau+T) \rangle \sim \alpha[(\alpha-1)/(\alpha+1)]\delta^{\alpha/2+3/2}T^{\alpha/2-3/2}$. Thus, even after a long period T a short perturbation still influences the process, and the sign of (2) depends on whether $\alpha \geq 1$. For $\alpha = 1$ (2) is zero, as expected. An example for the scaling behavior of the response function is shown in Fig. S7 in SM [76].

In fact, MMFBM (1) is formally similar to definitions in continuous and discrete time of multifractional FBM (MFBM) [77–80], a diverse family of processes based on a deterministic $\alpha(t)$ [81, 82]. MFBM and dedicated testing algorithms [83, 84] is used to describe data traffic dynamics [85, 86], financial time series [87], turbulent dynamics [88], or consumer index dynamics [89]. In most MFBM formulations, it is of interest to describe the roughness of trajectories and have a globally changing scaling exponent of the MSD. This is achieved by replacing $\alpha(s)$ in (1) by $\alpha(t)$, i.e., the Wiener increments $dB(s)$ at time t are modulated by the same exponent throughout the “history”. When $\alpha(t)$ changes, the memory of the correlations is reset and globally replaced by a new weight [90]. The changes of $\alpha(t)$ in MFBM directly affect the MSD, which scales as $\langle x^2(t) \rangle \simeq t^{\alpha(t)}$. This can be directly seen when calculating the response function: for MFBM (2) is identically zero, i.e., the reset of the history in MFBM kills any influence of the perturbation even at short periods T . We discuss further differences between MMFBM and MFBM below, arguing that MMFBM reflects memory properties expected for long-range correlated dynamics with uninterrupted memory.

Step-wise $\alpha(t)$ -protocol. To simplify the discussion of the general properties of MMFBM, we consider a step-wise protocol between two values of α switching at $t = \tau$,

$$\alpha(t) = \begin{cases} \alpha_1, & t \leq \tau \\ \alpha_2, & t > \tau \end{cases}, \quad (3)$$

in an unbounded space. More complicated behaviors can be constructed as a sequence of values α_i . Smooth ver-

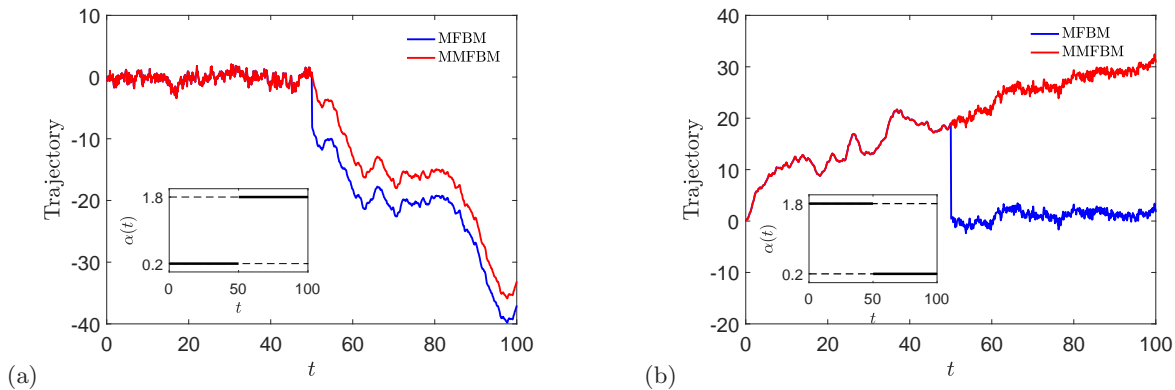


Figure 1: Sample trajectories for MMFBM (1) (red) and MFBM (S6) (blue) for step-like protocol (3) for $\alpha(t)$ with switching time $\tau = 50$ and (a): $\alpha_1 = 0.2$, $\alpha_2 = 1.8$; (b): $\alpha_1 = 1.8$, $\alpha_2 = 0.2$. In each panel both trajectories are based on the same realization of the parental Wiener process. For smooth protocol $\alpha(t)$ see Fig. S1. On a log-log scale the behavior for smooth and step-like protocol generally appear quite similar. Note the disparate behavior for $t > \tau$ in panel (b), see discussion below.

sions of the step-like protocol (3) can, e.g., be realized by sigmoid functions (S19) [76]. Such forms, however, require numerical analysis. Fig. 1 shows trajectories of MMFBM for the step-like form (3), while Fig. S1 depicts the case of a smooth protocol [76]. In both Figures we also show the corresponding MFBM trajectories, for the same parental Wiener processes $B(s)$. For both processes the roughness change in the trajectories at $t = \tau$ is distinct. In both cases MMFBM appears more “continuous”.

MSD. With definition (1), the MMFBM-MSD reads

$$\langle X^2(t) \rangle = \int_0^t \alpha(s)(t-s)^{\alpha(s)-1} ds, \quad (4)$$

due to the independence of the Wiener process at different times. Indeed, the instantaneous value of the MSD depends on the local modulation by $\alpha(s)$ along the process history. For the stepwise protocol (3), the MSD reads

$$\langle X^2(t) \rangle = \begin{cases} t^{\alpha_1}, & t \leq \tau \\ t^{\alpha_1} - (t-\tau)^{\alpha_1} + (t-\tau)^{\alpha_2}, & t > \tau \end{cases} \quad (5)$$

This form contrasts the MFBM result, for which $\langle X^2(t) \rangle \propto t^{\alpha(t)}$ for all t , i.e., for step-change (3) of α the MSD scaling exponent changes abruptly from α_1 to α_2 at $t = \tau$: by memory reset, at time t the history of the previous memory exponents at $s < t$ is erased in MFBM [76, 81, 82]. We note that in MMFBM even for stepwise $\alpha(t)$ considered here, the MSD is continuous at $t = \tau$ (the derivative is continuous for strong memory, $\alpha_1, \alpha_2 > 1$).

The MSD (5) already shows the interesting property that after the switching point $t = \tau$, both α_1 and α_2 appear. Expanding the MSD at long time $t \gg \tau$, we find

$$\langle X^2(t) \rangle \sim (\alpha_1 \tau) t^{\alpha_1-1} + t^{\alpha_2}. \quad (6)$$

Fig. 2 shows the time dependence of the MMFBM-MSD for both step-like and sigmoid protocols, showing perfect agreement with the predicted asymptotic behavior. In

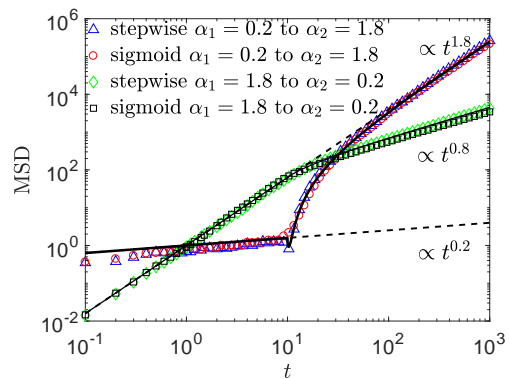


Figure 2: MSD for MMFBM $X(t)$ (1) for step-like and smooth protocol $\alpha(t)$ for two combinations of α_1 and α_2 (see legend). Full lines represent Eq. (5), symbols represent stochastic simulations. A comparison with MFBM is shown in Fig. S2 [76].

(6), as long as $\alpha_2 > \alpha_1 - 1$, the second exponent will eventually dominate the MSD scaling. As shown in SM [76], this convergence can, however, be very slow, much longer than the switching time τ . Even more, when $\alpha_1 > 1 + \alpha_2$ the MSD exhibits a continued scaling with $\alpha_1 - 1$ (as confirmed in Fig. 2). In other words, the more superdiffusive behavior is dominant asymptotically, albeit with the reduced slope $\alpha - 1$.

ACVF. We now study the ACVF, which is defined as

$$C(t, \Delta) = \langle X^\delta(t) X^\delta(t + \Delta) \rangle \quad (7)$$

with the increments $X^\delta(t) = X(t + \delta) - X(t)$. First we consider short t , i.e., the first increment $X^\delta(t)$ in (7) is taken before the switching time τ of $\alpha(t)$ in (3). Obviously, when also $t + \Delta < \tau$, the ACVF is the same as for RL-FBM with exponent α_1 and MFBM (Eq. (S12) [76]). This result explicitly depends on both t and Δ , due to

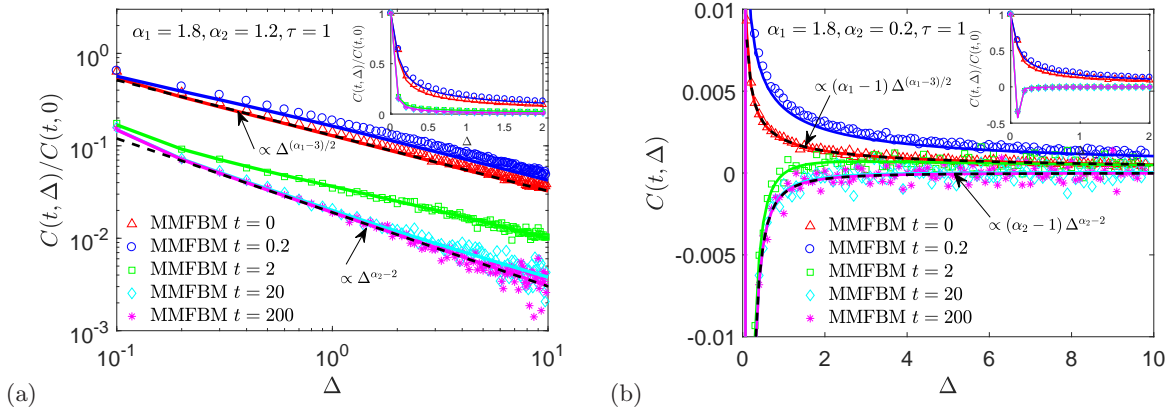


Figure 3: Numerical evaluations (lines) and simulations (symbols) for the ACVF $C(t, \Delta)$ at different times for MMFBM (1) with switching time $\tau = 1$ (a): $\alpha_1 = 1.8, \alpha_2 = 1.2$; (b): $\alpha_1 = 1.8, \alpha_2 = 0.2$. The inset in panel (b) shows the numerically obtained form close to $\Delta = 0$, demonstrating the antipersistence at long times t , when $\alpha_2 = 0.2$ becomes the dominant contribution. Note that in the main panel (b) the ACVF is shown in non-normalized form for better visibility.

the non-stationarity of RL-FBM. When $t = 0$ and $\delta \ll \tau$,

$$C(0, \Delta)_{\Delta < \tau} \sim \frac{\alpha_1(\alpha_1 - 1)\delta^{(\alpha_1+3)/2}}{\alpha_1 + 1} \Delta^{(\alpha_1-3)/2}. \quad (8)$$

Interestingly, when we correlate increments from before and after the switching time τ , $t + \Delta > \tau$, the MFMBM-ACVF (S11) depends on both α_1 and α_2 , while for MMFBM the ACVF is exactly that of *unswitched* RL-FBM and solely depends on α_1 . I.e., for $t = 0$ we recover the form (8) with $\Delta > \tau$. In fact, this result is not surprising. MFMBM after the switching is fully independent of the process before the switching, and thus both exponents occur in the ACVF. For MMFBM, in contrast, the process right after the switching event is still dominated by the memory from the evolution before the switching. Consequently, the sole occurrence of α_1 is indeed meaningful. At intermediate times, the MMFBM-ACVF depends on both α_1 and α_2 , as expected (see (S13)). The result needs to be evaluated numerically. However, in the limit $t \rightarrow \infty$, we expect the ACVF to forget about its history and solely depend on α_2 , which is indeed fulfilled,

$$C(\infty, \Delta) = \frac{\alpha_2(\alpha_2 - 1)\Gamma^2((\alpha_2 + 1)/2)\delta^2}{2\Gamma(\alpha_2)\sin(\pi\alpha_2/2)} \Delta^{\alpha_2-2}. \quad (9)$$

Fig. 3 depicts different scenarios for the ACVF (7). Nice agreement between stochastic simulations and the theoretical results is observed. Fig. S3 shows further cases. We also highlight the difference of the ACVF between the two models when t is close to the switching time τ but long lag times Δ are chosen in SM IV.C [76].

PDF. The PDF $P_1(x, t)$ of MMFBM for $t \leq \tau$ is Gaussian. To compute the PDF $P_2(x, t)$ after the crossover, we separate the process into two parts, that are both

Gaussian. The PDF of the full process is obtained as

$$P(x, t) = \frac{\exp(-x^2/[2(t^{\alpha_1} - (t-\tau)^{\alpha_1} + (t-\tau)^{\alpha_2}]])}{\sqrt{2\pi(t^{\alpha_1} - (t-\tau)^{\alpha_1} + (t-\tau)^{\alpha_2})}}, \quad (10)$$

which is again a Gaussian process. MMFBM remains Gaussian for any protocol $\alpha(t)$ of the memory exponent.

Local regularity. The self-similarity of a process determines its fractal (Hausdorff) graph dimension [91]. For a Gaussian process it is determined by the semivariogram (structure function) $\gamma_t(\delta) = \langle (X^\delta(t))^2 \rangle$. When $\gamma_t(\delta) \sim D_t \delta^\alpha$, the fractal graph dimension is $2 - \alpha/2$. This also holds for non-stationary increment processes such as RL-FBM [92]. For MMFBM with protocol (3) for $t < \tau$, $X(t)$ is identical to RL-FBM, so this part of the trajectory has fractal dimension $2 - \alpha_1/2$. After the switch it can be shown that the trajectory has fractal dimension $2 - \alpha_2/2$. For any graph containing a piece before and after τ , the lower fractional index and thus the higher fractal dimension dominates [93].

Conclusions. FBM is a widely used process to describe anomalous diffusion in soft- and bio-matter systems. It is characterized by long-ranged, positive or negative correlations in time. Yet many real-world systems exhibit changes in the anomalous diffusion exponent (and thus the memory exponent modulating the correlations in the motion) as function of time. Prime examples include environments, in which particles cross between areas of different viscoelastic properties or when the degree of crowding is controlled. Cargo being pulled intermittently by molecular motors switch between sub- and superdiffusion in cells, and search strategies of birds with correlated increments may vary over time as they switch their motion mode in response to the environment, time of day, or season. Tracers in fluidic setups that modulate between effectively three- and two-dimensional embedding should

change the exponent of the power-law Basset force. In finance the instantaneous degree of roughness of the trading data may vary during the daily rhythm, following interventions in the market, or due to longer-lasting events such as pandemics, wars, or vacation times. Long-range correlated processes such as viscoelastic anomalous diffusion necessarily feature effects of memory of the entire dynamics in physical observables such as the MSD or the ACVF, both of which can be measured.

We here introduced MMFBM as a generalization of FBM to a deterministic form $\alpha(t)$ of the memory exponent. In the correlation integral $\alpha(s)$ locally modulates the Wiener increments $dB(s)$ and thus contributes to the correlation history of the process. The MSD, and the ACVF of MMFBM exhibit crossovers carrying explicit information from the process prior to switching. This contrasts MFBM, which resets the previous history globally, as seen in the MSD $\langle x^2(t) \rangle \simeq t^{\alpha(t)}$, that solely depends on the instantaneous value of α at process time t . While this reset of correlation history is irrelevant when discussing the instantaneous roughness of a trajectory, for a physical process with long-range correlations this point is crucial when the correlations are directly probed, e.g., in single particle tracking experiments. Here, MMFBM appears physically consistent. We hope that MMFBM will find wide use in soft- and bio-matter systems, finance, ecology, etc. MMFBM will also extend the arsenal of generalized stochastic processes in data analysis [35, 36].

Our discussion was based on non-stationary RL-FBM. MMFBM is thus useful for the description of typical physical systems initiated at $t = 0$ that first have to equilibrate. We demonstrated that at sufficiently long times asymptotic stationarity is restored. It will be interesting to see how MMFBM is modified in the fully stationary limit, i.e., generalizing Mandelbrot-van Ness FBM for systems, that are equilibrated at the start of the measurement. We note that apart from using a purely time-dependent protocol $\alpha(t)$ corresponding to deterministic modifications of the system, it will be interesting to consider scenarios of space-varying scaling exponents in a heterogeneous, quenched system, as well as to combine a protocol $\alpha(t)$ with a time dependence of the (generalized) diffusion coefficients as observed in [49]. Moreover, non-Gaussian extensions of MMFBM should be studied, as well as effects of cutoffs or tempering [94] of the correlations. Finally it should be studied how the non-standard behavior of FBM [95, 96] next to boundaries is modified for MMFBM, relevant, e.g., for growing serotonergic fibers in inhomogeneous brain environments [97].

We acknowledge support from German Science Foundation (DFG grant ME 1535/12-1) and NSF-BMBF CRCNS (grant 2112862/STAXS). AVC acknowledges support by the Polish National Agency for Academic Exchange (NAWA). AW was supported by the Polish National Center of Science (Opus 2020/37/B/HS4/00120). KB acknowledges support through Beethoven Grant

DFG-NCN 2016/23/G/ST1/04083.

-
- [1] C. Manzo and M. F. Garcia-Parajo, A review of progress in single particle tracking: from methods to biophysical insights, *Rep. Prog. Phys.* **78**, 124601 (2015).
 - [2] E. Barkai, Y. Garini, and R. Metzler, Strange kinetics of single molecules in living cells, *Phys. Today* **65**(8), 29 (2012).
 - [3] M. J. Saxton, Anomalous subdiffusion in fluorescence photobleaching recovery: a Monte Carlo study, *Biophys. J.* **81**, 2226 (2001).
 - [4] F. Höfling and T. Franosch, Anomalous transport in the crowded world of biological cells, *Rep. Prog. Phys.* **76**, 046602 (2013).
 - [5] J. Szymanski and M. Weiss, Elucidating the origin of anomalous diffusion in crowded fluids, *Phys. Rev. Lett.* **103**, 038102 (2009).
 - [6] J.-H. Jeon, N. Leijnse, L. B. Oddershede, and R. Metzler, Anomalous diffusion and power-law relaxation of the time averaged mean squared displacement in worm-like micellar solutions, *New J. Phys.* **15**, 045011 (2013).
 - [7] S. C. Weber, A. J. Spakowitz, and J. A. Theriot, Bacterial chromosomal loci move subdiffusively through a viscoelastic cytoplasm, *Phys. Rev. Lett.* **104**, 238102 (2010).
 - [8] T. J. Lampo, S. Stylianidou, M. P. Backlund, P. A. Wiggins, and A. J. Spakowitz, Cytoplasmic RNA-protein particles exhibit non-Gaussian subdiffusive behavior, *Biophys. J.* **112**, 532 (2017).
 - [9] J.-H. Jeon et al., *In Vivo* Anomalous Diffusion and Weak Ergodicity Breaking of Lipid Granules, *Phys. Rev. Lett.* **106**, 048103 (2011).
 - [10] M. Magdziarz, A. Weron, K. Burnecki and J. Klafter, Fractional Brownian motion versus the continuous-time random walk: A simple test for subdiffusive dynamics, *Phys. Rev. Lett.* **103**, 180602 (2009).
 - [11] I. Bronstein et al., Transient anomalous diffusion of telomeres in the nucleus of mammalian cells, *Phys. Rev. Lett.* **103**, 018102 (2009).
 - [12] A. Caspi, R. Granek, and M. Elbaum., Enhanced diffusion in active intracellular transport, *Phys. Rev. Lett.* **85**, 5655 (2000).
 - [13] G. Seisenberger et al., Real-time single-molecule imaging of the infection pathway of an adeno-associated virus, *Science* **294**, 1929 (2001).
 - [14] K. J. Chen, B. Wang, and S. Granick, Memoryless self-reinforcing directionality in endosomal active transport within living cells, *Nature Mat.* **14**, 589 (2015).
 - [15] A. V. Weigel, B. Simon, M. M. Tamkun, and D. Krapf, Ergodic and nonergodic processes coexist in the plasma membrane as observed by single-molecule tracking, *Proc. Natl. Acad. Sci. USA* **108**, 6438 (2011).
 - [16] W. He et al., Dynamic heterogeneity and non-Gaussian statistics for acetylcholine receptors on live cell membrane, *Nat. Comm.* **7**, 11701 (2016).
 - [17] C. Manzo et al., Weak ergodicity breaking of receptor motion in living cells stemming from random diffusivity, *Phys. Rev. X* **5**, 011021 (2015).
 - [18] M. J. Skaug, L. Wang, Y. Ding, and D. K. Schwartz, Hindered nanoparticle diffusion and void accessibility in

- a three-dimensional porous medium, *ACS Nano* **9**, 2148 (2015).
- [19] J.-H. Jeon, H. Martinez-Seara Monne, M. Javanainen, and R. Metzler, Anomalous diffusion of phospholipids and cholesterol in a lipid bilayer and its origins, *Phys. Rev. Lett.* **109**, 188103 (2012).
- [20] J.-H. Jeon, M. Javanainen, H. Martinez-Seara, R. Metzler, and I. Vattulainen, Protein crowding in lipid bilayers gives rise to non-Gaussian anomalous lateral diffusion of phospholipids and proteins, *Phys. Rev. X* **6**, 021006 (2016).
- [21] E. Yamamoto, T. Akimoto, A. Mitsutake, and R. Metzler, Universal relation between instantaneous diffusivity and radius of gyration of proteins in aqueous solution, *Phys. Rev. Lett.* **126**, 128101 (2021).
- [22] X. Hu, L. Hong, M. Dean Smith, T. Neusius, and J. C. Smith, The dynamics of single protein molecules is non-equilibrium and self-similar over thirteen decades in time, *Nature Phys.* **12**, 171 (2016).
- [23] S. Hapca, J. W. Crawford, and I. M. Young, Anomalous diffusion of heterogeneous populations characterized by normal diffusion at the individual level, *J. R. Soc. Interface* **6**, 111 (2009).
- [24] K. C. Leptos, J. S. Guasto, J. P. Gollub, A. I. Pesci, and R. E. Goldstein, Dynamics of enhanced tracer diffusion in suspensions of swimming eukaryotic microorganisms, *Phys. Rev. Lett.* **103**, 198103 (2009).
- [25] A. G. Cherstvy, O. Nagel, C. Beta, and R. Metzler, Non-Gaussianity, population heterogeneity, and transient superdiffusion in the spreading dynamics of amoeboid cells, *Phys. Chem. Chem. Phys.* **20**, 23034 (2018).
- [26] N. E. Humphries et al., Environmental context explains Lévy and Brownian movement patterns of marine predators, *Nature* **465**, 1066 (2010).
- [27] D. W. Sims, N. E. Humphries, N. Hu, V. Medan, and J. Berni, Optimal searching behaviour generated intrinsically by the central pattern generator for locomotion, *eLife* **8**, e50316 (2019).
- [28] R. Nathan et al., *Science* **375**, Big-data approaches lead to an increased understanding of the ecology of animal movement, eabg1780 (2022).
- [29] O. Vilck et al., Ergodicity breaking in area-restricted search of avian predators, *Phys. Rev. X* **12**, 031005 (2022).
- [30] O. Vilck et al., Unravelling the origins of anomalous diffusion: from molecules to migrating storks, *Phys. Rev. Res.* **4**, 033055 (2022).
- [31] N. G. van Kampen, *Stochastic processes in physics and chemistry* (North Holland, Amsterdam, 1981).
- [32] J.-P. Bouchaud and A. Georges, Anomalous diffusion in disordered media: statistical mechanisms, models and physical applications, *Phys. Rep.* **195**, 127 (1990).
- [33] R. Metzler, J.-H. Jeon, A. G. Cherstvy, and E. Barkai, Anomalous diffusion models and their properties: non-stationarity, non-ergodicity, and ageing at the centenary of single particle tracking, *Phys. Chem. Chem. Phys.* **16**, 24128 (2014).
- [34] I. M. Sokolov, Models of anomalous diffusion in crowded environments, *Soft Matter* **8**, 9043 (2012).
- [35] G. Muñoz-Gil et al., Objective comparison of methods to decode anomalous diffusion, *Nature Comm.* **12**, 6253 (2021).
- [36] H. Seckler and R. Metzler, Bayesian deep learning for error estimation in the analysis of anomalous diffusion, *Nat. Commun.* **13**, 6717 (2022).
- [37] M. Levin, G. Bel, and Y. Roichman, Measurements and characterization of the dynamics of tracer particles in an actin network, *J. Chem. Phys.* **154**, 144901 (2021).
- [38] I. Y. Wong et al., Anomalous diffusion probes microstructure dynamics of entangled F-actin networks, *Phys. Rev. Lett.* **92**, 178101 (2004).
- [39] A. Díez Fernandez, P. Charchar, A. G. Cherstvy, R. Metzler, and M. W. Finnis, The diffusion of doxorubicin drug molecules in silica nanoslits is non-Gaussian, intermittent and anticorrelated, *Phys. Chem. Chem. Phys.* **22**, 27955 (2020).
- [40] M. S. Song, H. C. Moon, J.-H. Jeon, and H. Y. Park, Neuronal messenger ribonucleoprotein transport follows an aging Lévy walk, *Nature Comm.* **9**, 344 (2018).
- [41] T. H. Solomon, E. R. Weeks, and H. L. Swinney, Observation of anomalous diffusion and Lévy flights in a two-dimensional rotating flow, *Phys. Rev. Lett.* **71**, 3975 (1993).
- [42] T. Geisel and S. Thomae, Anomalous diffusion in intermittent chaotic systems, *Phys. Rev. Lett.* **52**, 1936 (1984).
- [43] A. N. Kolmogorov, Wiener'sche spiralen und einige andere interessante kurven in hilbertscher raum, *C. R. (Doklady)*, *Acad. Sci. URSS (N. S.)* **26**, 115 (1940).
- [44] B. B. Mandelbrot and J. W. van Ness, Fractional Brownian motions, fractional noises and applications, *SIAM Rev.* **10**, 422 (1968).
- [45] H. Qian, in *Processes with long-range correlations: theory and applications*, edited by G. Rangarajan and M. Z. Ding, *Lecture Notes in Physics* vol 621 (Springer, New York, 2003).
- [46] W. H. Deng and E. Barkai, Ergodic properties of fractional Brownian-Langevin motion, *Phys. Rev. E* **79**, 011112 (2009).
- [47] J. F. Reverey et al., Superdiffusion dominates intracellular particle motion in the supercrowded cytoplasm of pathogenic *Acanthamoeba castellanii*, *Sci. Rep.* **5**, 11690 (2015).
- [48] D. Krapf et al., Spectral content of a single non-Brownian trajectory, *Phys. Rev. X* **9**, 011019 (2019).
- [49] A. Sabri, X. Xu, D. Krapf, and M. Weiss, Elucidating the origin of heterogeneous anomalous diffusion in the cytoplasm of mammalian cells, *Phys. Rev. Lett.* **125**, 058101 (2020).
- [50] Z. R. Fox, E. Barkai, and D. Krapf, Aging power spectrum of membrane protein transport and other subordinated random walks, *Nat. Comm.* **12**, 6162 (2021).
- [51] B. J. Alder and T. E. Wainwright, Decay of the velocity autocorrelation function, *Phys. Rev. A* **1**, 18 (1970).
- [52] A. Mcdonough, S. P. Russo, and I. K. Snook, Long-time behavior of the velocity autocorrelation function for moderately dense, soft-repulsive, and Lennard-Jones fluids, *Phys. Rev. E* **63**, 026109 (2001).
- [53] G. L. Paul and P. N. Pusey, Observation of a long-time tail in Brownian motion, *J. Phys. A* **14**, 3301 (1981).
- [54] T. Franosch, M. Grimm, M. Belushkin, F. M. Mor, G. Foffi, L. Forro, and S. Jeney, Resonances arising from hydrodynamic memory in Brownian motion, *Nature* **478**, 7367 (2011).
- [55] F. Comte and E. Renault, Long memory in continuous-time stochastic volatility models, *Math. Fin.* **8**, 291 (1998).

- [56] J. Gatheral, T. Jaisson, and M. Rosenbaum, Volatility is rough, *Quant. Fin.* **18**, 933 (2018).
- [57] B. Wang, J. Kuo, S. C. Bae, and S. Granick, When Brownian diffusion is not Gaussian, *Nat. Mater.* **11**, 481 (2012).
- [58] Y. Lanoiselée, N. Moutal, and D. S. Grebenkov, Diffusion-limited reactions in dynamic heterogeneous media, *Nat. Commun.* **9**, 4398 (2018).
- [59] J. Słezak, R. Metzler, and M. Magdziarz, Superstatistical generalised Langevin equation: non-Gaussian viscoelastic anomalous diffusion, *New J. Phys.* **20**, 023026 (2018).
- [60] A. V. Chechkin, F. Seno, R. Metzler, and I. M. Sokolov, Brownian yet non-Gaussian diffusion: from superstatistics to subordination of diffusing diffusivities, *Phys. Rev. X* **7**, 021002 (2017).
- [61] M. V. Chubynsky and G. W. Slater, Diffusing diffusivity: a model for anomalous, yet Brownian, diffusion, *Phys. Rev. Lett.* **113**, 098302 (2014).
- [62] W. Wang et al., Fractional Brownian motion with random diffusivity: emerging residual nonergodicity below the correlation time, *J. Phys. A* **53**, 474001 (2020).
- [63] W. Wang, F. Seno, I. M. Sokolov, A. V. Chechkin, and R. Metzler, Unexpected crossovers in correlated random-diffusivity processes, *New J. Phys.* **22**, 083041 (2020).
- [64] D. Han et al., Deciphering anomalous heterogeneous intracellular transport with neural networks, *elife* **9**, e52224 (2020).
- [65] M. Balcerk, K. Burnecki, S. Thapa, A. Wyłomańska, and A. Chechkin, Fractional Brownian motion with random Hurst exponent: Accelerating diffusion and persistence transitions, *Chaos* **32**, 093114 (2022).
- [66] P. D. Odermatt et al. Variations of intracellular density during the cell cycle arise from tip-growth regulation in fission yeast, *eLife* **10**, 64901 (2021).
- [67] A. J. Barlow et al., The effect of pressure on the viscoelastic properties of liquids, *Proc. Roy. Soc. A* **327**, 403 (1972).
- [68] J. Caspers et al., How are mobility and friction related in viscoelastic fluids? E-print arXiv:10820.0122.
- [69] F. Etoc et al., Non-specific interactions govern cytosolic diffusion of nanosized objects in mammalian cells, *Nat. Mat.* **17**, 740 (2018).
- [70] I. Heller et al., STED nanoscopy combined with optical tweezers reveals protein dynamics on densely covered DNA, *Nat. Meth.* **10**, 910 (2013).
- [71] D. Robert, T. Nguyen, F. Gallet, and C. Wilhelm, In vivo determination of fluctuating forces during endosome trafficking using a combination of active and passive microrheology, *PLoS ONE* **5**, e10046 (2010).
- [72] I. Goychuk, V. O. Kharchenko, and R. Metzler, Molecular motors pulling cargos in the viscoelastic cytosol: power strokes beat subdiffusion, *Phys. Chem. Chem. Phys.* **16**, 16524 (2014).
- [73] P. Lévy, in *Random functions: general theory with special reference to Laplacian random functions* (University of California Press, Berkeley, 1953).
- [74] We here use a dimensionless notation. To restore physical units the associated prefactor $\alpha(s)$ in Eq. (1) can be replaced by the form $[K_{\alpha(s)}] = \alpha(s)\ell_0^2/t_0^{\alpha(s)}$. Dimensionality can then be removed by setting the length scale ℓ_0 and the time scale t_0 to unity. The specific choice of the dimensionless prefactor $\alpha(s)$ in this expression for $K_{\alpha(s)}$ allows a compact notation and to illustrate the most essential features of the MMFBM model.
- [75] A. V. Chechkin, R. Gorenflo, and I. M. Sokolov, Retarding subdiffusion and accelerating superdiffusion governed by distributed-order fractional diffusion equations, *Phys. Rev. E* **66**, 046129 (2002).
- [76] Supplementary Material
- [77] A. Ayache, C. Esser, and J. Hamonier, A new multifractional process with random exponent, *Risk Decis. Anal.* **7**, 5 (2018).
- [78] A. Philippe, D. Surgailis, and M.-C. Viano, Time-varying fractionally integrated processes with nonstationary long memory, *Theory Prob. Appl.* **52**, 651 (2008).
- [79] D. Surgailis, Nonhomogeneous fractional integration and multifractional processes, *Stoch. Proc. Appl.* **118**, 171 (2008).
- [80] A. Ayache and F. Bouly, Moving average Multifractional Processes with Random Exponent: lower bounds for local oscillations, *Stoch. Proc. Appl.* **146**, 143 (2022).
- [81] S. A. Stoev and M. S. Taqqu, How rich is the class of multifractional Brownian motions?, *Stoch. Proc. Appl.* **116**, 200 (2006).
- [82] A. Ayache and J. Lévy-Vehel, The generalized multifractional Brownian motion, *Statist. Infer. Stoch. Proc.* **3**, 7 (2000).
- [83] M. Balcerk and K. Burnecki, Testing of multifractional Brownian motion, *Entropy* **22**, 1403 (2020).
- [84] D. Szarek, I. Jabłoński, D. Krapf, and A. Wyłomańska, Multifractional Brownian motion characterization based on Hurst exponent estimation and statistical learning, *Chaos* **32**, 083148, (2022).
- [85] M. Li, S. C. Lim, B.-J. Hu, and H. Feng, in *Lecture notes in computer science 4488*, edited by Y. Shi, G. Dick van Albada, J. Dongarra, and P. M. A. Sloot (Springer, Berlin, 1987).
- [86] J. Lévy-Vehel and R. Riedi, in *Fractals in engineering*, edited by J. Lévy Véhel, E. Lutton, and C. Tricot (Springer, Berlin, 1997).
- [87] S. Bianchi, A. Pantanella, and A. Pianese, Modeling stock prices by multifractional Brownian motion: an improved estimation of the pointwise regularity, *Quant. Fin.* **13**, 1317 (2011).
- [88] K. C. Lee, Characterization of turbulence stability through the identification of multifractional Brownian motions, *Nonlin. Proc. Geophys.* **20**, 97 (2013).
- [89] C. Box, Multifractional Brownian motion and its applications to factor analysis on consumer confidence index, Senior thesis, Claremont College, 2021.
- [90] We note that we choose the additional prefactor $\sqrt{\alpha(t)}$ in the definition of MFBM, compare [77] in agreement with RL-FBM [44]. This choice does not change the fundamental behavior.
- [91] K. Falconer, *Fractal geometry* (John Wiley & Sons, Chichester, UK, 1990).
- [92] J. Picard, in *Séminaire de Probabilités XLIII*, edited by C. Donati-Martin, A. Lejay, and A. Rouault, *Lecture Notes in Mathematics 2006* (Springer, New York, 2011).
- [93] W. Wang et al., (unpublished).
- [94] D. Molina-Garcia et al., Crossover from anomalous to normal diffusion: truncated power-law noise correlations and applications to dynamics in lipid bilayers, *New J. Phys.* **20**, 103027 (2018).
- [95] T. Vojta et al., Reflected fractional Brownian motion in one and higher dimensions, *Phys. Rev. E* **102**, 032108

- (2020).
- [96] T. Guggenberger, A. Chechkin, and R. Metzler, Fractional Brownian motion in superharmonic potentials and non-Boltzmann stationary distributions, *J. Phys. A* **54**, 29LT01 (2021).
 - [97] S. Janušonis, N. Detering, R. Metzler, and T. Vojta, Serotonergic axons as fractional Brownian motion paths: insights into the self-organization of regional densities, *Front. Comp. Neurosci.* **14**, 56 (2020).
 - [98] M. Abramowitz and I. Stegun, *Handbook of mathematical functions* (Dover, New York, 1972).

Supplementary Material:
Memory-multi-fractional Brownian motion with continuous correlations

LÉVY'S RIEMANN-LIOUVILLE-FBM

A well-known representation of fractional Brownian motion (FBM) is attributed by Mandelbrot [44] to Paul Lévy [73]. It is given by the Holmgren-Riemann-Liouville fractional integral [44]

$$B_\alpha(t) = \sqrt{\alpha} \int_0^t (t-s)^{(\alpha-1)/2} dB(s) \quad (\text{S1})$$

$B(t)$ is standard Brownian motion and $\alpha \in (0, 2]$. It is easy to show that the MSD of $B_\alpha(t)$ yields as $\langle B_\alpha^2(t) \rangle = t^\alpha$.

This exact equality follows from the choice of the prefactor in definition (S1) [65].

With the increments of RL-FBM for disjoint intervals $[t, t + \delta]$ and $[t + \Delta, t + \Delta + \delta]$,

$$B_\alpha^\delta(t) = B_\alpha(t + \delta) - B_\alpha(t), \quad B_\alpha^\delta(t + \Delta) = B_\alpha(t + \Delta + \delta) - B_\alpha(t + \Delta), \quad (\text{S2})$$

the ACVF of RL-FBM is given by

$$C_B(t, \Delta) = \langle B_\alpha^\delta(t) B_\alpha^\delta(t + \Delta) \rangle. \quad (\text{S3})$$

For $\Delta \gg \delta$, after some transformations we obtain the ACVF

$$\begin{aligned} C_B(t, \Delta) &\approx \frac{\alpha(\alpha-1)(3-\alpha)\delta^2}{4} \int_0^t q^{(\alpha-1)/2} (q+\Delta)^{(\alpha-5)/2} dq + \frac{\alpha(\alpha-1)\delta}{2} \int_t^{t+\delta} q^{(\alpha-1)/2} (q+\Delta)^{(\alpha-3)/2} dq \\ &= \frac{\alpha(\alpha-1)(3-\alpha)\delta^2}{4} \text{B}\left(\frac{t/\Delta}{1+t/\Delta}; \frac{\alpha+1}{2}, 2-\alpha\right) \Delta^{\alpha-2} + \frac{\alpha(\alpha-1)\delta}{2} \int_t^{t+\delta} q^{(\alpha-1)/2} (q+\Delta)^{(\alpha-3)/2} dq, \end{aligned} \quad (\text{S4})$$

where $\text{B}(z; a, b)$ is the incomplete Beta function [98]

$$\text{B}(z; a, b) = \int_0^z s^{a-1} (1-s)^{b-1} ds. \quad (\text{S5})$$

RL-FBM has non-stationary increments at any given time t , i.e., it does not solely depend on the time lag Δ .

MFBM

A direct generalization of FBM to multifractional Brownian motion (MFBM) is to replace α by an explicitly time-dependent function $\alpha(t)$. In comparison to mathematical literature (see, e.g., [77, 81, 82]) we base the generalization on RL-FBM (S1) with the square-root prefactor,

$$Y(t) = \sqrt{\alpha(t)} \int_0^t (t-s)^{(\alpha(t)-1)/2} dB(s). \quad (\text{S6})$$

In MFBM, the long-range correlations are reset, as only the instantaneous value of α at time t is considered in (S6), and the MSD scales like

$$\langle Y^2(t) \rangle = t^{\alpha(t)}. \quad (\text{S7})$$

Trajectories for MFBM and MMFBM for the step-like protocol (3) are shown in Fig. 1, and for a smooth protocol in Fig. S1. While for the smooth protocol the discontinuity seen in Fig. 1 is remedied, the general shape of the trajectories in both cases are quite similar.

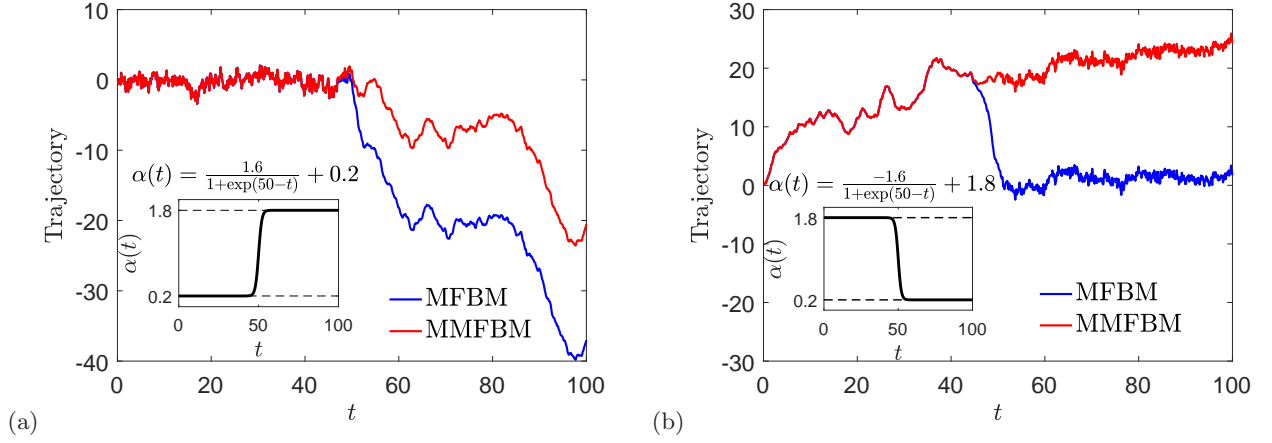


Figure S1: Trajectories for MMFBM (1) and MFBM (S6) for a smooth protocol (S19) for $\alpha(t)$ with switching time $\tau = 50$ and (a): $\alpha_1 = 0.2, \alpha_2 = 1.8$; (b): $\alpha_1 = 1.8, \alpha_2 = 0.2$. In each panel both trajectories are based on the same realization of the underlying Wiener process. The time series of the parental Wiener increments is also the same as for Fig. 1, in which we show trajectories produced by a step-like protocol (2).

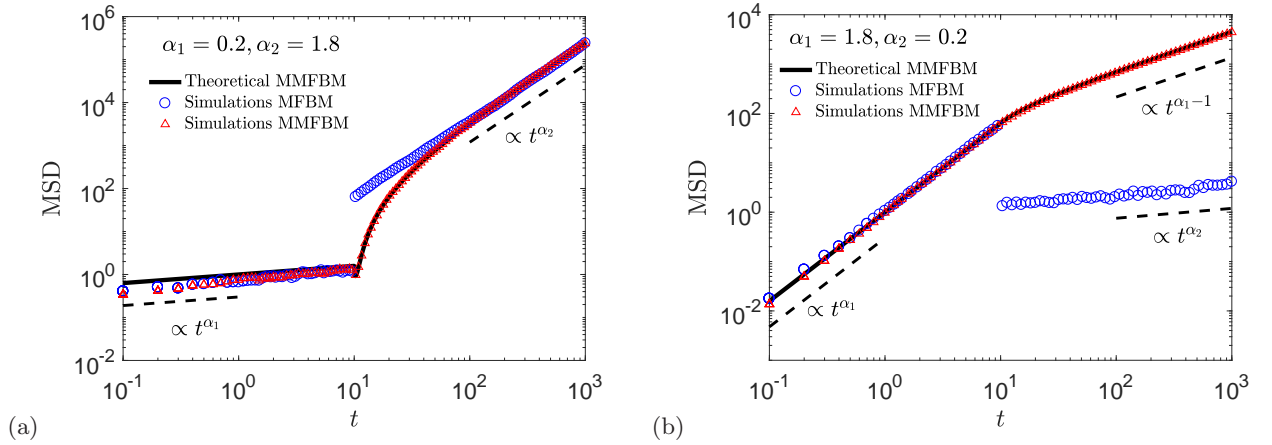


Figure S2: MSDs for MFB and MMFBM with switching time $\tau = 10$: (a) $\alpha_1 = 0.2, \alpha_2 = 1.8$, (b) $\alpha_1 = 1.8, \alpha_2 = 0.2$. The theoretical MSD (5) of MMFBM is represented by solid black curves. Note that the MMFBM-MSD is always continuous, while the derivative is continuous when $\alpha_1, \alpha_2 > 1$. For MFBM the MSD is always discontinuous.

MSD OF MFBM

The MSD of MFBM (S6) with step-like anomalous diffusion exponent jumping from α_1 to α_2 at $t = \tau$, yields in the form

$$\langle Y^2(t) \rangle = \begin{cases} t^{\alpha_1}, & t \leq \tau \\ t^{\alpha_2}, & t > \tau \end{cases} \quad (\text{S8})$$

Indeed, for $t > \tau$, solely the value α_2 appears, due to the reset correlations of MFBM. The MSDs for MFBM and MMFBM are displayed in Fig. S2 along with stochastic simulations.

ACVF FOR MMFBM AND MFBM

We define the increment of MMFBM as $X^\delta(t) = X(t + \delta) - X(t)$. The ACVF is given by $C_X(t, \Delta) = \langle X^\delta(t) X^\delta(t + \Delta) \rangle$, where the time step δ is taken to be small, $\delta \ll \Delta, \tau$. Similarly, the ACVF for MFBM

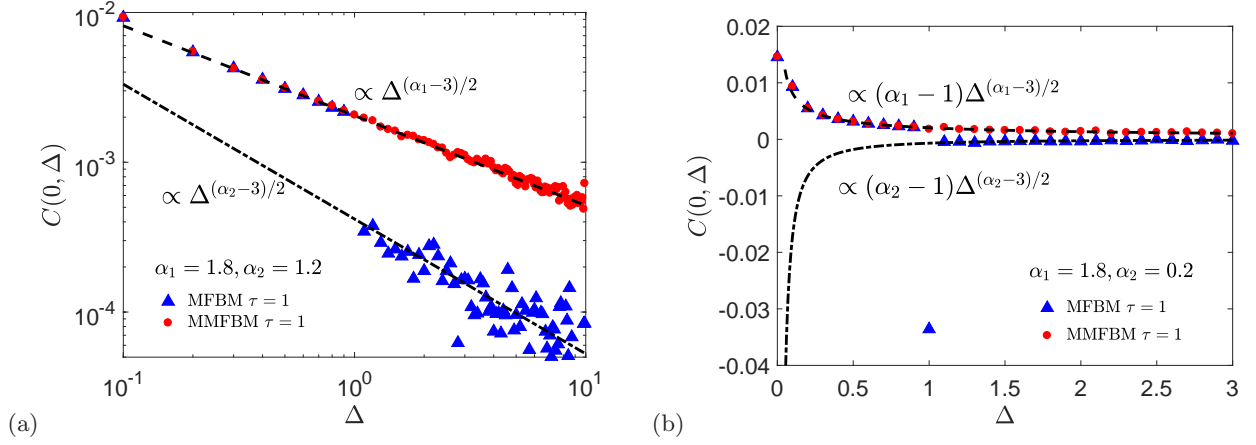


Figure S3: ACVF for MFBM and MMFBM with switching time $\tau = 1$. The theoretical ACVF of classic MFBM (S9) switches to (S12) when the anomalous diffusion exponent switches. The ACVF $C(0, \Delta)$ of MMFBM (S9), (S10) remains the same depending on α_1 .

(S6) is $C_Y(t, \Delta)$. In the limits of short and long times t analytical results can be obtained for the ACVFs for step-like protocol of α .

Short time limit of the ACVF

We first consider $t < \tau$. Then we distinguish two cases:

- (i) When $t + \Delta < \tau$ we have the same ACVF (S4) as that of RL-FBM. In particular, when $t = 0$ and $\Delta \gg \delta$, we have the ACVF for both MMFBM and MFBM according to

$$C_X(0, \Delta)_{\Delta < \tau} = C_Y(0, \Delta)_{\Delta < \tau} = C_B(0, \Delta | \alpha_1) \sim \frac{\alpha_1(\alpha_1 - 1)\delta^{(\alpha_1+3)/2}}{\alpha_1 + 1} \Delta^{(\alpha_1-3)/2}. \quad (\text{S9})$$

- (ii) When $t + \Delta > \tau$, the increment $X^\delta(t + \Delta)$ of MMFBM is measured after switching and $X^\delta(t)$ before switching. Multiplying the two increments and averaging over the realizations, the ACVF is independent of α_2 and coincides with the results (S4) of RL-FBM. For $t = 0$ and $\Delta \gg \delta$,

$$C_X(0, \Delta)_{\Delta > \tau} \sim \frac{\alpha_1(\alpha_1 - 1)\delta^{(\alpha_1+3)/2}}{\alpha_1 + 1} \Delta^{(\alpha_1-3)/2}. \quad (\text{S10})$$

In contrast, for MFBM the increment after switching is given by $Y(t + \Delta + \delta) - Y(t + \Delta)$ and the ACVF for MFBM depends on both α_2 and α_1 ,

$$C_Y(t, \Delta)_{t+\Delta > \tau} = \frac{\sqrt{\alpha_1 \alpha_2}(\alpha_2 - 1)(3 - \alpha_2)\delta^2}{4} \text{B} \left(\frac{t/\Delta}{1 + t/\Delta}; \frac{\alpha_1 + 1}{2}, 2 - \frac{\alpha_1 + \alpha_2}{2} \right) \Delta^{(\alpha_1 + \alpha_2)/2 - 2} \\ + \frac{\sqrt{\alpha_1 \alpha_2}(\alpha_2 - 1)\delta}{2} \int_t^{t+\delta} q^{(\alpha_1-1)/2} (q + \Delta)^{(\alpha_2-3)/2} dq. \quad (\text{S11})$$

When $t = 0$ and $\Delta \gg \delta$, we have the MFBM-ACVF

$$C_Y(0, \Delta)_{\Delta > \tau} \sim \frac{\sqrt{\alpha_1 \alpha_2}(\alpha_2 - 1)\delta^{(\alpha_1+3)/2}}{\alpha_1 + 1} \Delta^{(\alpha_2-3)/2}. \quad (\text{S12})$$

The ACVF of MMFBM and MFBM are shown in Fig. S3. When the anomalous diffusion exponent switches from α_1 to α_2 , the ACVF for $t = 0$ of MFBM crosses over from the scaling $\Delta^{(\alpha_1-3)/2}$ to $\Delta^{(\alpha_2-3)/2}$, while the MMFBM-ACVF retains the scaling $\Delta^{(\alpha_1-3)/2}$. This clearly shows the uninterrupted memory of MMFBM, in contrast to MFBM.

Long time limit of the ACVF

When $t > \tau$ both increments are observed after the switching of α . After some transformations we obtain the ACVF

$$C_X(t, \Delta) = f\left(\alpha_1, \frac{t}{\Delta}\right) - f\left(\alpha_1, \frac{t-\tau}{\Delta}\right) + f\left(\alpha_2, \frac{t-\tau}{\Delta}\right) + g\left(\alpha_1, \frac{t}{\Delta}\right) - g\left(\alpha_1, \frac{t-\tau}{\Delta}\right) + g\left(\alpha_2, \frac{t-\tau}{\Delta}\right), \quad (\text{S13})$$

where

$$f(\alpha, s) = \frac{\alpha(\alpha-1)\delta^2}{2} s^{(\alpha-1)/2} (1+s)^{(\alpha-3)/2} \Delta^{\alpha-2}, \quad g(\alpha, s) = \frac{\alpha(\alpha-1)(3-\alpha)\delta^2}{4} \text{B}\left(\frac{s}{1+s}; \frac{\alpha+1}{2}, 2-\alpha\right) \Delta^{\alpha-2}. \quad (\text{S14})$$

When $t \rightarrow \infty$,

$$C_X(\infty, \Delta) = g(\alpha_2, \infty) = \frac{\alpha_2(\alpha_2-1)\Gamma^2((\alpha_2+1)/2)\delta^2}{2\Gamma(\alpha_2)\sin(\pi\alpha_2/2)} \Delta^{\alpha_2-2}. \quad (\text{S15})$$

For MFBM, the increments depend locally on the Hurst exponents at time t . The ACVF of MFBM is the same as that of FBM with the same α_2 at time t after switching, and when $t \rightarrow \infty$,

$$C_Y(\infty, \Delta) = \frac{\alpha_2(\alpha_2-1)\Gamma^2((\alpha_2+1)/2)\delta^2}{2\Gamma(\alpha_2)\sin(\pi\alpha_2/2)} \Delta^{\alpha_2-2}. \quad (\text{S16})$$

As it should be, at extremely long times beyond the switching time, the ACVFs of RL-FBM, MFBM, and MMFBM converge to the same behavior.

Long lag time limit of ACVF for times around the switching time

We finally consider the limit of long lag times, $\Delta \gg t$, while the time t is taken to be close to the switching time, $t \gtrsim \tau$. As the incomplete Beta function $\text{B}(s; a, b) \sim s^a/a$ when $s \ll 1$, the function $g(\alpha, s) \simeq s^{(\alpha+1)/2} \Delta^{\alpha-2}$ with $s = t/\Delta$ or $s = (t-\tau)/\Delta$ in Eq. (S13) can be neglected in comparison with $f(\alpha, s)$, and one can approximate the ACVF as

$$C_X(t, \Delta) \sim d_1 \Delta^{(\alpha_1-3)/2} + d_2 \Delta^{(\alpha_2-3)/2}, \quad (\text{S17})$$

where $d_1 = \frac{1}{2}\alpha_1(\alpha_1-1)\delta^2(t^{(\alpha_1-1)} - (t-\tau)^{(\alpha_1-1)})$ and $d_2 = \frac{1}{2}\alpha_2(\alpha_2-1)\delta^2(t-\tau)^{(\alpha_2-1)}$. Thus the ACVF is a combination of two scaling behaviors $\Delta^{(\alpha_1-3)/2}$ and $\Delta^{(\alpha_2-3)/2}$. The former scaling is inherited from before the switching, i.e., is caused by the memory of MMFBM, and the latter emerges with the instantaneous exponent after switching. In Fig. S4, the combination of the scaling of the ACVF is shown by the green dashed curves. For the case in the left panel of Fig. S4, the intermediate-scaling behavior predicted by Eq. (S17) is close to the simulated behavior. In the right panel, the minimum of the ACVF is not captured well, however, we see convergence at sufficiently long lag times.

In contrast to MMFBM, the ACVF of MFBM solely depends on the instantaneous exponent α_2 and is given by

$$C_Y(t, \Delta) = C_B(t, \Delta|\alpha_2) \sim \frac{\alpha_2(\alpha_2-1)\Gamma^2((\alpha_2+1)/2)\delta^2}{2\Gamma(\alpha_2)\sin(\pi\alpha_2/2)} \Delta^{\alpha_2-2}, \quad (\text{S18})$$

where $C_B(t, \Delta|\alpha_2)$ is the ACVF of RL-FBM with exponent α_2 .

Simulations for both $C_X(t, \Delta)$, Eq. (S17), and $C_Y(t, \Delta)$, Eq. (S18), around switching time are represented by the green symbols in Fig. S4. We note that the simulations at long lag time Δ in the right panel exhibit more pronounced fluctuations due to the subdiffusive behaviors after switching.

SMOOTH SWITCHING OF ANOMALOUS DIFFUSION EXPONENT

While the stepwise protocol (2) used here simplifies the analytical calculation, it is interesting to consider smooth variations. We here briefly study the exponentially switching anomalous diffusion exponent

$$\alpha(t) = \frac{\alpha_2 - \alpha_1}{1 + \exp\left(- (t - \tau)/T\right)} + \alpha_1, \quad (\text{S19})$$

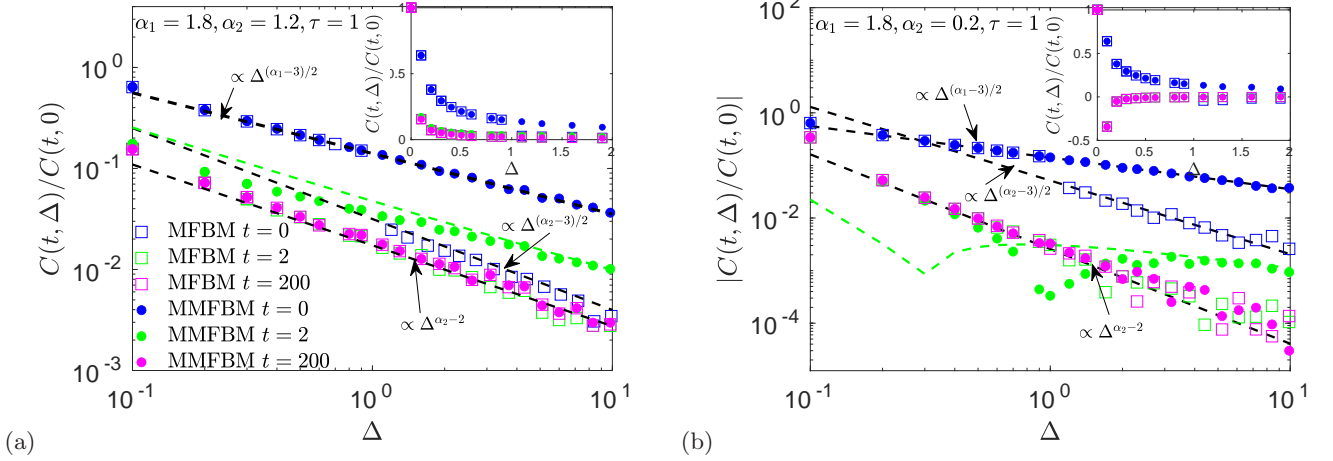


Figure S4: Simulations of the ACVFs for MFBM and MMFBM with switching time $\tau = 1$ and (a) $\alpha_1 = 1.8, \alpha_2 = 1.2$, (b) $\alpha_1 = 1.8, \alpha_2 = 0.2$. The ACVF of MFBM with $t = 0$ is discontinuous at the switching time τ and switches to $\Delta^{(\alpha_2-3)/2}$ from $\Delta^{(\alpha_1-3)/2}$ (blue squares). In contrast, the ACVF of MMFBM is always continuous with scaling $\Delta^{(\alpha_1-3)/2}$ (blue circles), demonstrating the influence of the memory from the process before switching. The ACVF of MFBM at around the switching time $t \approx \tau$ solely depends on instantaneous the exponent α_2 (green squares), Eq. (S18), while the ACVF of MMFBM depends on both α_1 and α_2 (green circles) with the long lag time behaviors given by the combination the two scaling behaviors in Eq. (S17) (green curves). The ACVFs converge at long time t to the scaling Δ^{α_2-2} .

where T is some characteristic time measuring how fast the exponent switches from α_1 to α_2 around $t = \tau$. At short times $t \ll \tau$, we see that $\alpha(t) \approx \alpha_1$ while at long times $t \gg \tau$, $\alpha(t) \approx \alpha_2$. Numerically evaluated trajectories and MSDs for MFBM and MMFBM with smoothly switching exponent (S19) are displayed in Figs. S1 and 2.

PHYSICALLY ASYMPTOTIC BEHAVIOR

As we showed in the main text, a new scaling of the MSD of MMFBM with the power-law t^{α_1-1} emerges at long times when the memory before switching is strong, $\alpha_1 > \alpha_2 + 1$. Otherwise, when this inequality is not fulfilled, the MSD of MMFBM converges to MFBM in the mathematically asymptotic limit $t \rightarrow \infty$. The natural question that arises: what is the physically measurable time scale, after which the MSDs of the two models converge? The physical time scale to compare with is given by the switching time $t = \tau$. To reveal the characteristic time for the convergence of the two MSDs, we test the ratio of the difference of the MSDs of the two models (MMFBM Eq. (1) and MFBM Eq. (S6)) to that of MFBM at time $t \gg \tau$,

$$\begin{aligned} \text{Error} &= \frac{\langle X^2(t) \rangle - \langle Y^2(t) \rangle}{\langle Y^2(t) \rangle} = \frac{(t^{\alpha_1} - (t-\tau)^{\alpha_1} + (t-\tau)^{\alpha_2}) - t^{\alpha_2}}{t^{\alpha_2}} \\ &\sim \frac{\alpha_1 \tau}{t^{1+\alpha_2-\alpha_1}} - \frac{\alpha_2 \tau}{t}. \end{aligned} \quad (\text{S20})$$

This allows us to distinguish three cases:

- (i) When $\alpha_1 > \alpha_2 + 1$, the relative deviation of the MSD of MMFBM to MFBM grows with the power $t^{\alpha_1-\alpha_2-1}$. In this case, the MMFBM never converges to MFBM at long times. Instead, the new scaling t^{α_1-1} of the MSD emerges, which corresponds to Eq. (6) and is shown in Fig. 2 in the main text.
- (ii) When $\alpha_2 < \alpha_1 < \alpha_2 + 1$, the ratio (S20) decays to zero with power $t^{-(1+\alpha_2-\alpha_1)}$ (an example is shown in Fig. (S5)) and the MSD of MMFBM starts to converge to MFBM after a time scale $\tau^{1/(1+\alpha_2-\alpha_1)}$. This time scale can become much longer than τ as $1/(1+\alpha_2-\alpha_1) > 1$, where we note that in our dimensionless units, the time scale $\tau \gg 1$, as unity represents the elementary diffusive step.
- (iii) When $\alpha_2 > \alpha_1$, the ratio (S20) decays to zero with power t^{-1} , and the MSD of MMFBM starts to converge to MSD after a time scale which is equivalent to τ .

We provide simulation results for cases (ii) and (iii) to validate the physical limiting time observed for different choices of the exponents. In Fig. S5 the much slower convergence of case (ii) is distinct. It is thus necessary to go to extremely long times to observe the pure α_2 -scaling of MFBM. For practical, physical applications such scales can

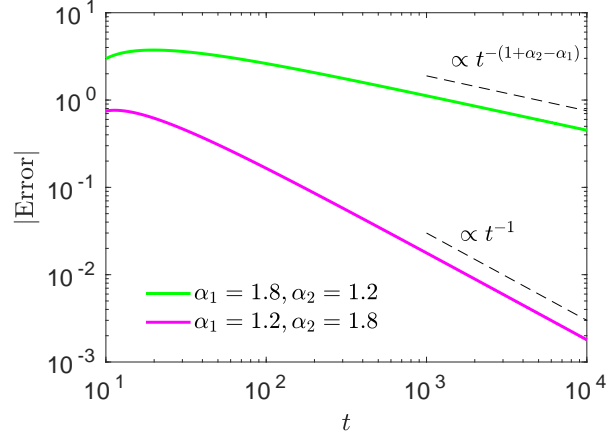


Figure S5: Error (S20) of the MSD from MMFBM to MFBM. While for $\alpha_1 < \alpha_2 + 1$ the two models converge in the mathematical limit $t \rightarrow \infty$, the speed of convergence is very different for cases (ii) and (iii). Namely, when $\alpha_2 < \alpha_1$, the deviation between MMFBM and MFBM is dominated by the slower power-law $t^{-(1+\alpha_2-\alpha_1)}$, whereas for $\alpha_2 > \alpha_1$ the error decays to zero with the faster power-law t^{-1} .

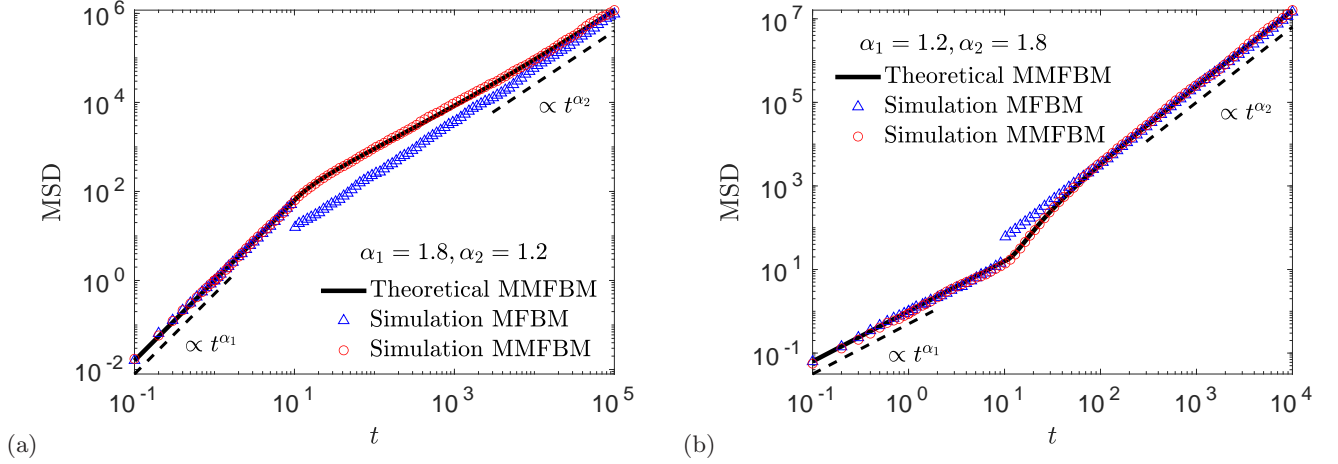


Figure S6: MSDs for MMFBM and MFBM with switching time $\tau = 10$. The theoretical MSDs, Eq. (5) in the main text, are represented by the full lines. In the left panel, the MSD of MMFBM starts to converge to MFBM when $t \geq \tau^{1/(1+\alpha_2-\alpha_1)} \approx 316$, much longer than the switching time $\tau = 10$, while in the right panel the convergence time is equivalent to the switching time $\tau = 10$.

rarely be reached, and it is thus relevant to consider the memory contained in MMFBM. We also show the MSD-convergence for two examples in Fig. S6. For the case (ii) in the left panel, several orders of magnitude in time need to be measured to observe convergence of the MMFBM result to that of MFBM.

RESPONSE FUNCTION

In Fig. S7 we show an example for the response function.

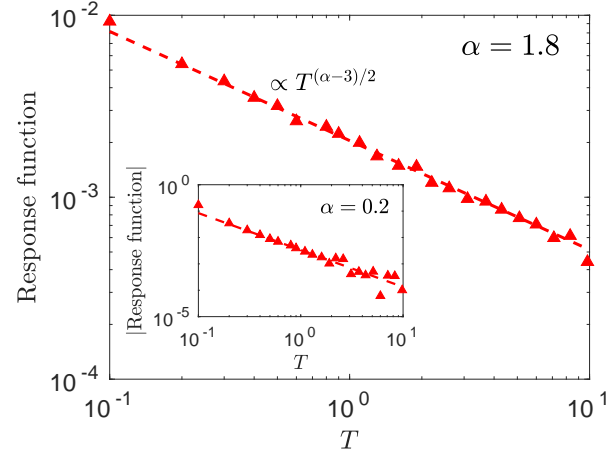


Figure S7: Response function for MMFBM with switching time $\tau = 1$. The dashed curves represent the exact response function, Eq. (2) in the main text. Unlike the response function of MFBM, which is always zero ($T > 0$), the response function of MMFBM decays with the power law $T^{(\alpha-3)/2}$.